Pergamon

Composites Engineering, Vol. 4, No. 9, pp. 947–964, 1994

0961-9526/94 $7.00+ .00

0961-9526(94) E00042-5

EFFECT OF FIBER LENGTH VARIATION ON TENSILE PROPERTIES OF CARBON-FIBER CEMENT COMPOSITES

Victor C. Li and Karthikeyan H. Obla

Advanced Civil Engineering Materials Research Laboratory, University of Michigan, Ann Arbor, MI 48109-2125, U.S.A.

(*Received* 28 *April* 1994; *final version accepted* 23 *May* 1994)

Abstract—Unlike other fiber types, carbon fibers tend to possess a distribution of fiber lengths even before mixing into a cementitious matrix. During mixing, some amount of fiber rupture may be expected. Along with other fiber parameters, fiber length distribution may be expected to play an important role in governing the composite properties. This paper describes the results of an experimental program which measures the length distribution of carbon fibers both before and after mixing. A database of composite tensile stress–strain behavior is established for a number of commercially available carbon fibers in a cementitious matrix. Special emphasis is placed on pseudo strain-hardening behavior and the associated ultimate tensile strength beyond first cracking. A theoretical model of this ultimate strength which explicitly account for fiber length distribution is developed and shown to account for the reduced tensile strength of experimentally observed results reasonably well. Results of this research suggest that for the purpose of brittle cementitious matrix reinforcement, carbon fibers with higher strain capacity may be more important than high modulus typically demanded for polymer matrix composite reinforcement.

1. INTRODUCTION

Carbon fibers do not corrode, have superior fire resistance and possess long-term durability in an alkaline medium such as cement paste, thus making them superior to steel, polymeric and glass fibers. With the development of pitch-based fibers and new processing routes, the cost of carbon fibers has reduced to a level which makes it economically viable as concrete reinforcement for civil engineering applications. However, the design of carbon-cement composites provides some unique challenges.

Carbon fibers cover a wide range of properties with strengths ranging between 400 and 5000 MPa, modulus varying between 7 and 400 GPa, and various surface finishes that can yield a wide range of bond-strength values (Akihama *et al.*, 1986; Ermolenko *et al.*, 1990; Park and Lee, 1993). Also, they can be made to have a range of diameters and can be cut to different lengths. When different carbon fibers are used to make cement composites they can be expected to yield different composite properties covering a wide range (Akihama *et al.*, 1984; Nishioka *et al.*, 1986; Linton *et al.*, 1991; Banthia *et al.*, 1994; Yang and Chung, 1992).

Carbon fibers are finer (6–20 μm in diameter) than most other fibers used for concrete reinforcement. They are also very brittle. Due to these reasons they tend to break when mixed with other concrete constituents in the mixer (Nishioka *et al.*, 1986; Linton *et al.*, 1991). The extent of fiber breakage during mixing depends upon the fiber parameters (such as strength, diameter, strain capacity, length), mixer type, mixing speed, mixing time and mix proportions (amount of aggregates etc.). Also, the carbon-fiber production technique tends to impart a length distribution on the fiber. This is particularly true for pitch fiber type. Due to the above reasons the actual fibers reinforcing the concrete composite tend to have a length distribution. Also, carbon fibers tend to break in the matrix when the composite is subjected to tensile loading if the tensile stress in the fiber exceeds its failure stress. This can happen if the fiber length is greater than the critical fiber length (Kelly and Macmillan, 1986).

In this paper, uniaxial tensile properties of cementitious composites reinforced with various commercially available carbon fibers are summarized. These tests are part of a larger experimental program investigating the design of carbon-fiber-reinforced cementitious composites at the University of Michigan. In the present work, focus is placed on

the influence of fiber length distribution on composite tensile strength. Evidence for fiber length variations before and after mixing is presented. Fiber length distribution is incorporated into a theoretical model of the composite bridging stress vs crack-opening relationship (σ-δ). This model also accounts for fiber rupture during crack opening. Model prediction of tensile strength is shown to agree reasonably well with experimental measurements. In contrast, an existing model which does not account for fiber length variation consistently overestimates the composite tensile strength. This result suggests that for fiber types which are brittle and/or have variable fiber length, such as carbon, composite properties are significantly influenced by tensile rupture and fiber length variation. These effects must be taken into account in the design of such composites.

2. EXPERIMENTAL PROGRAM

The objective of this experimental work is three-fold: (1) To create a database of uniaxial tensile behavior of cement composites using a variety of (five) commercially available carbon fibers. Not all fibers are manufactured for use in a cementitious composite. (2) To determine the fiber length variation before mixing and the extent of breakage during mixing of the different carbon fiber types. (3) To relate fiber mechanical and geometric properties to composite properties. In order to obtain a deeper level of understanding for this last objective, a theoretical model of composite tensile strength is developed which accounts for fiber rupture and fiber length variation. This model is described in Section 3 of this paper. Uniaxial tensile testing and fiber length distribution studies were conducted on all five sets of composites.

2.1. *Materials and processing*

The matrix used is a typical low w/c ratio cement-paste matrix (see Table 1 for details). An Omni mixer of 10 liter capacity was used for mixing the carbon-fiber cement composite as it has shown to display good mixing (Banthia, 1992). The mixing time was maintained at 4 min after fiber addition and the mixing speed was maintained at level 10. The casting of the carbon-fiber cement composite material was carried out using high-frequency vibration (120 Hz).

The specimens were covered with plastic sheets and stored for 24 hours. After 1 day the specimens were demolded and placed into water curing tanks at room temperature for 4 weeks. The specimens were taken out of the water and tested after 2 days of drying under normal laboratory conditions.

Five different fiber types were used (Table 2). The fiber length L_f, diameter d_f, tensile strength σ_{fu}, Young's modulus E_f, tensile strain capacity ε_{fu} and density ρ were obtained from the manufacturer's literature. The fiber/matrix interface bond strength τ and mean fiber length before mixing L_f^{bm} and after mixing L_f^{am} are determined in this experimental program and described in more detail later.

Table 1. Mix proportions

ASTM Type III cement	Condensed silica fume	Super-plasticizer (Melment)	Water
1.00	0.10	0.0133	0.31

Table 2. Fiber parameters of the different fibers used in the CFRC tensile test

Fiber type	L_f (mm)	d_f (μm)	σ_{fu} (MPa)	E_f (GPa)	ε_{fu} (%)	ρ (g cm^{-3})	τ (MPa)	L_f^{bm} (mm)	L_f^{am} (mm)	V_f (%)
F-1	6	6.8	4600	268	1.70	1.77	—	6.08	2.51	3.0
F-2	6	12	690	48	1.44	1.57	—	1.95	1.81	2.5
F-3	12	12	690	48	1.44	1.57	—	4.08	2.58	2.5
F-4	3	24	800	38	2.1	1.62	3.10	2.80	2.40	4.0
F-5	10	20	800	38	2.1	1.62	1.57	9.91	6.67	4.0

L_f = fiber length according to manufacturer's specification.
L_f^{bm} = measured average fiber length before mixing.
L_f^{am} = measured average fiber length after mixing.

2.2. *Uniaxial tension test*

The size of the tensile coupon specimen used in this test series was 304.8 × 76.2 × 12.7 mm. The coupon specimens were tested under displacement control in a 133.5 kN capacity MTS 810 material testing system with hydraulic wedge grips. The displacement rate used was 0.005 mm s^{-1}. Aluminum plates were glued onto the ends of the tension specimens to facilitate gripping. The MTS machine has a fully digital control panel and Teststar software to automatically run the tests and collect the data. In addition, two LVDTs hooked to the Labtech Notebook data acquisition system were used to measure displacements between two points on the specimen at a gage length of 205 mm. The uniaxial tensile behavior of the composite can then be determined from these tests. More details of the uniaxial tensile testing procedure are described in Li *et al.* (1994).

2.3. *Results of uniaxial tension tests*

The tensile stress–strain curves for the carbon cement composites are shown in Fig. 1. Composites reinforced with F-2 and F-3 fibers show a brittle mode of failure with a linear elastic ascending portion followed by a sudden drop in load-carrying capacity after the formation of the first crack. The tensile strengths observed were 4.53 and 5 MPa for composites reinforced with F-2 and F-3 fibers, respectively. In comparison, the plain cement matrix (which also failed in a brittle manner, as expected) has a tensile strength of 2 MPa. The composite reinforced with F-1 fibers shows a quasi-brittle mode of failure with a tensile strength of about 8 MPa. Composites reinforced with F-4 and F-5 fibers show a ductile mode of failure with tensile strengths of 7.10 and 8.20 MPa, respectively. In particular, the composite reinforced with F-5 fibers shows a high strain capacity of 0.90% (as much as 90 times that of the plain cement matrix). This material demonstrates that pseudo strain hardening (Li and Leung, 1992; Marshall and Cox, 1988) can be achieved with carbon fibers.

The curves shown in Fig. 1 are representative test results of three or more repeated tests. However, variability (e.g. of 20–30% in tensile strength) does exist, as for most uniaxial tensile tests of brittle-matrix composites.

2.4. *Experimental study of fiber length distribution*

The extent of fiber breakage during mixing depends upon the fiber parameters—fiber strength, diameter, length and strain capacity. High fiber breakage during mixing can be expected from a fiber of low strength, small diameter, long length and low strain capacity. Fiber breakage may increase with the amount of aggregates in the matrix, although this aspect is not studied here. Fiber breakage might also vary with the mixer type, mixing time and mixing speed. The Omni mixer without any internal blades should lead to reduced fiber breakage during mixing as compared to a mixer with blades.

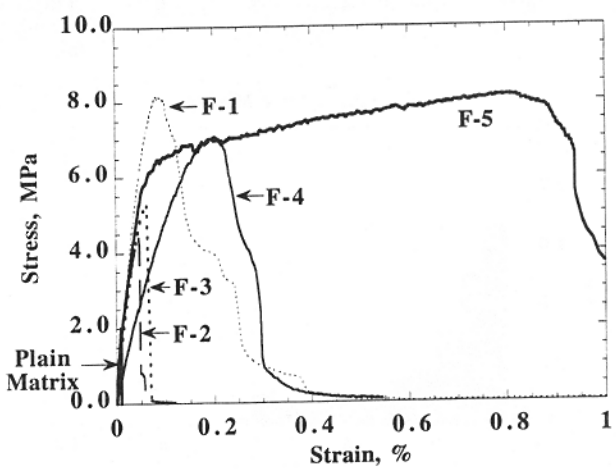

Fig. 1. Uniaxial tensile test results of various commercially available carbon-fiber cement composites.

The extent of fiber breakage has been observed for each fiber type after mixing. Since only the fiber parameters are varied in this experiment, it is possible to compare the extent of breakage during mixing of the different fiber types individually.

2.4.1. *Measurement of fiber length distribution.* Before mixing, a small sample of fibers was separated for length distribution measurements. After mixing with the cement paste a small sample of the fresh composite mix was placed on a 75 μm sieve. Water was passed through the sieve at a very slow speed for a period of approximately 10 min. At this point all the cement paste would have been washed off and the fibers in the wet condition were allowed to dry under normal laboratory conditions for a day.

The fiber samples were spread out on a white background. Digitized images of the fiber samples were captured using a low-power microscope/camera of magnification about 20×. Using image-analysis software, the individual fiber lengths were measured. Several images were taken and the lengths of at least 300 fibers were included for each fiber type in order to get an accurate estimate of fiber length of a statistically significant population.

2.4.2. *Results of fiber length measurement.* Figures 2 and 3 show computerized images of fiber length distributions of F-1 fibers before and after mixing, and F-2 fibers before mixing, respectively. Fiber length distributions for all fibers are shown in Figs 4–8 as fiber counts. The average fiber lengths before mixing L_f^{bm} and after mixing L_f^{am} are reported in Table 2. Specific observations from examination of these figures are given below:

(1) According to the manufacturer's specifications, F-1 and F-2 fibers are of 6 mm length. This can be readily confirmed from Fig. 2a for F-1 fibers. However, Fig. 3 shows that the fibers of F-2 vary between 0.38 and 9 mm with an average length of 1.95 mm. Therefore it can be said that some fibers (F-1, F-4, F-5—refer to Figs 2a, 4a, 7a, 8a) have an almost uniform fiber length (small variation) before mixing, whereas other fibers (F-2, F-3—refer to Figs 3, 5a, 6a) have fiber lengths

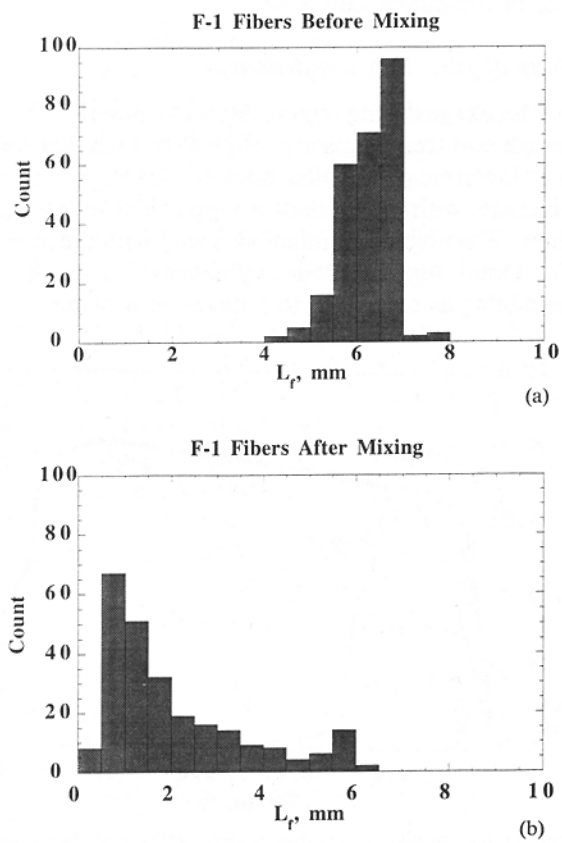

Fig. 4. Measured fiber length distribution of F-1 fibers (a) before mixing, and (b) after mixing.

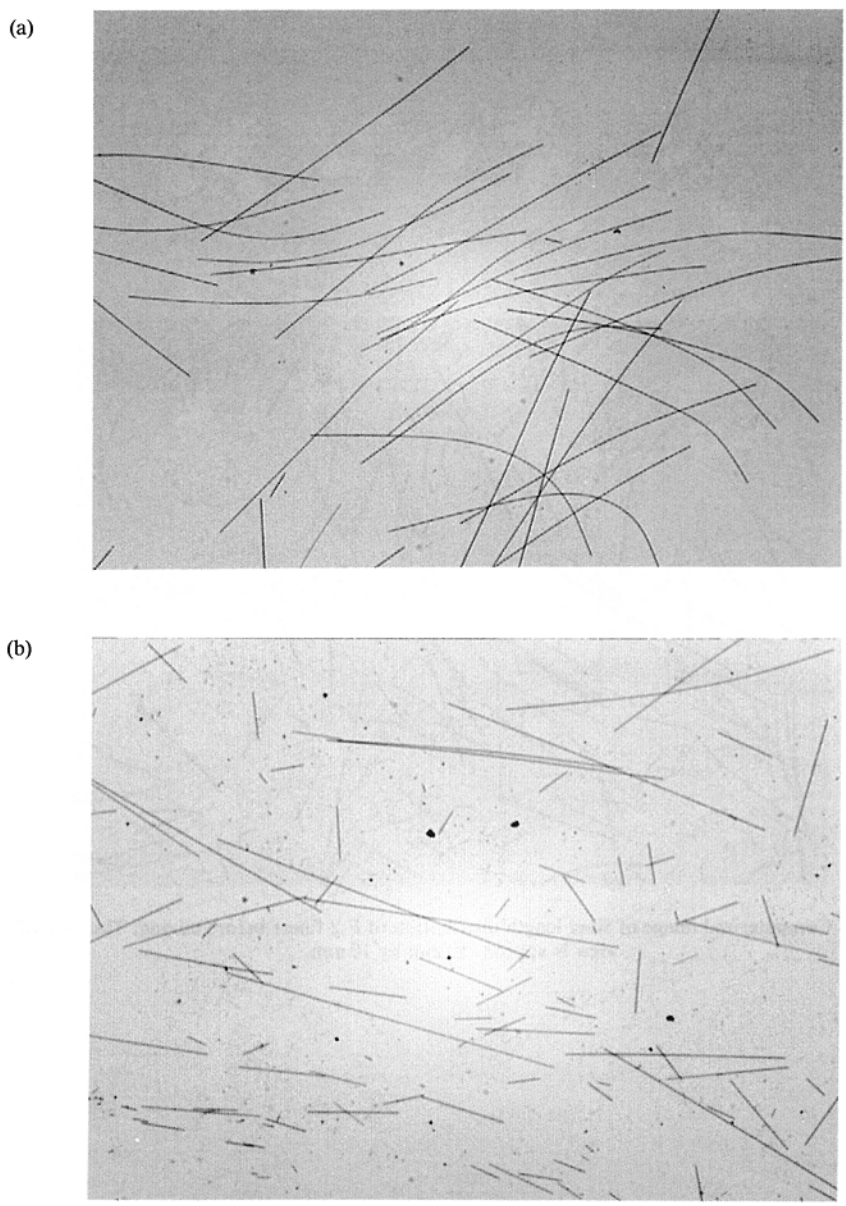

Fig. 2. Computerized image of fiber length distribution of F-1 fibers (a) before mixing, and (b) after mixing. The field of view is approx. 10 mm by 10 mm.

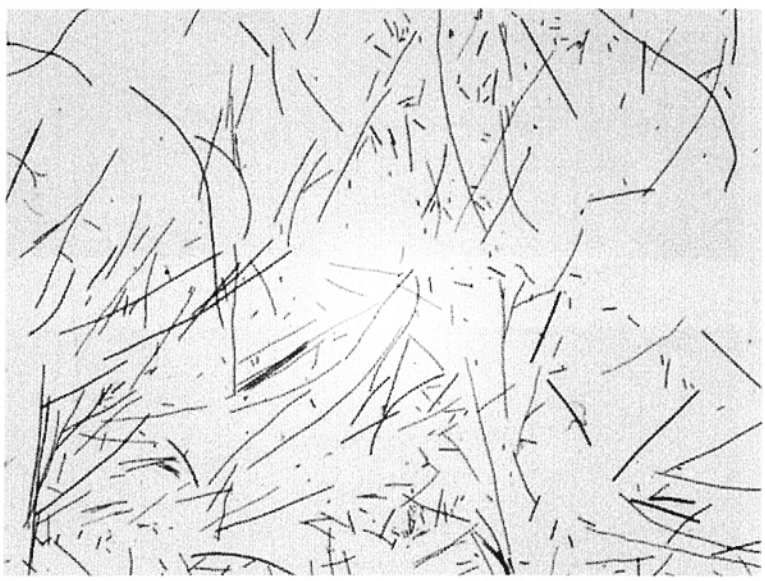

Fig. 3. Computerized image of fiber length distribution of F-2 fibers before mixing. The field of view is approx. 10 mm by 10 mm.

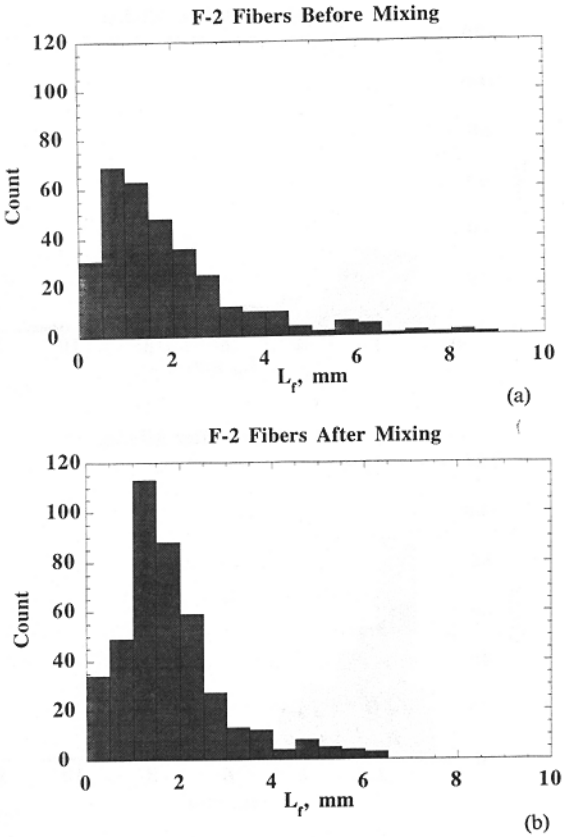

Fig. 5. Measured fiber length distribution of F-2 fibers (a) before mixing, and (b) after mixing.

with high variations even before mixing. However, note that a constant fiber length before mixing is *not a requirement* to obtain good composite properties.

(2) F-1 fibers, which started with an average original length of 6.08 mm, broke down during mixing to give an average length of 2.51 mm, a reduction of nearly 60% (Figs 2, 4). This could be due to their higher aspect ratio (1000 compared to less than 500 for the other fibers, see Table 2 for more details of fiber properties) inspite of their high strength. This suggests that fiber aspect ratio plays a much more crucial role in determining the extent of fiber breakage during mixing.

(3) F-4 fibers have a manufacturer-specified length of 3 mm. During mixing the fiber broke down from an average fiber pre-mix length of 2.80 mm to about 2.40 mm (15% reduction—Fig. 7). F-5 fibers have a manufacturer-specified length of 10 mm. During mixing the fiber broke down from an average length of 9.91 mm to about 6.67 mm (30% reduction—Fig. 8). The increased breakage of F-5 fibers could be due to two factors—a longer pre-mix length of 9.91 mm, and a slightly smaller diameter (20 vs 24 μm).

(4) The mean values of length distribution for F-2 fibers (1.95 mm) and F-3 fibers (4.08 mm) before mixing are substantially lower than the manufacturer's specified length of 6 and 12 mm, respectively.

The measured L_f distribution after mixing of the different fiber types has been approximated by mathematical equations which are used as the probability density functions of fiber lengths $p(L_f)$ for the different fiber types (Fig. 9). The average fiber length for each $p(L_f)$ is made consistent with the average fiber length after mixing. These $p(L_f)$ expressions are used in the analytical model (Section 3) to predict the tensile strengths of composites made with those fiber types. The predicted composite tensile strengths are compared with experimental results from uniaxial tensile tests.

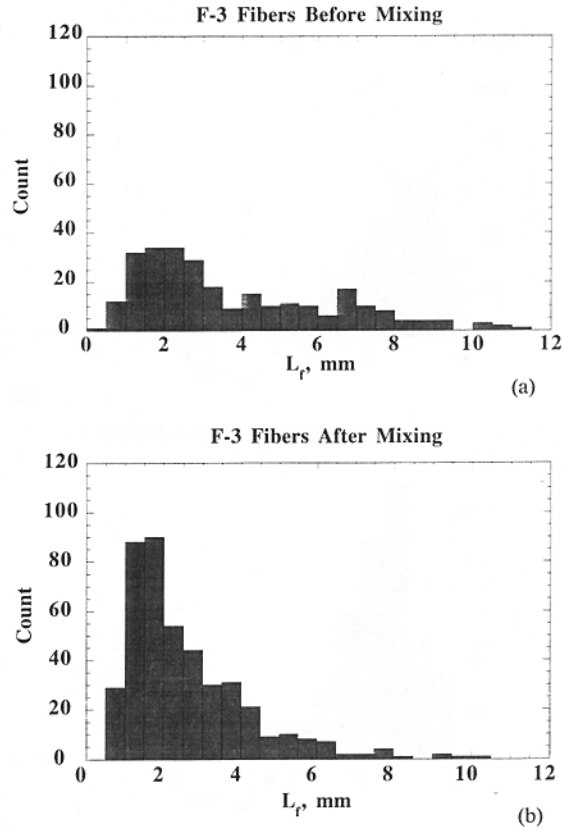

Fig. 6. Measured fiber length distribution of F-3 fibers (a) before mixing, and (b) after mixing.

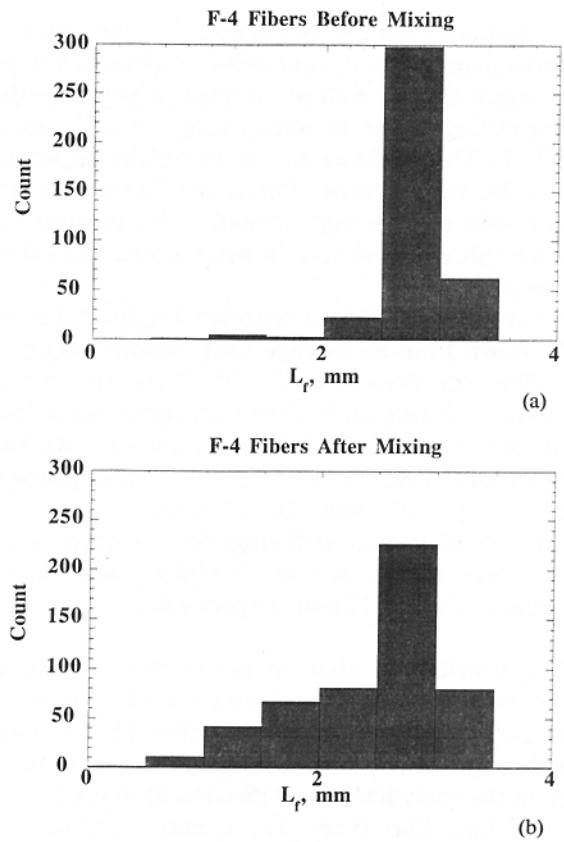

Fig. 7. Measured fiber length distribution of F-4 fibers (a) before mixing, and (b) after mixing.

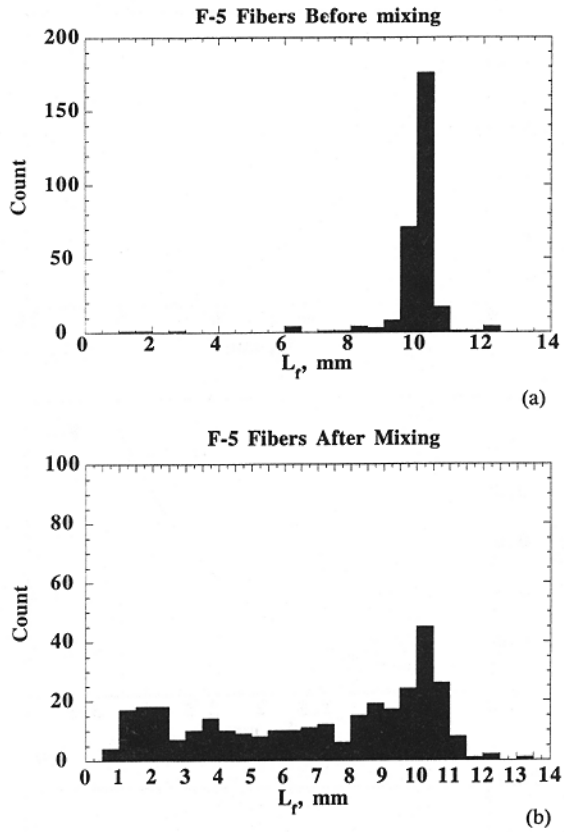

Fig. 8. Measured fiber length distribution of F-5 fibers (a) before mixing, and (b) after mixing.

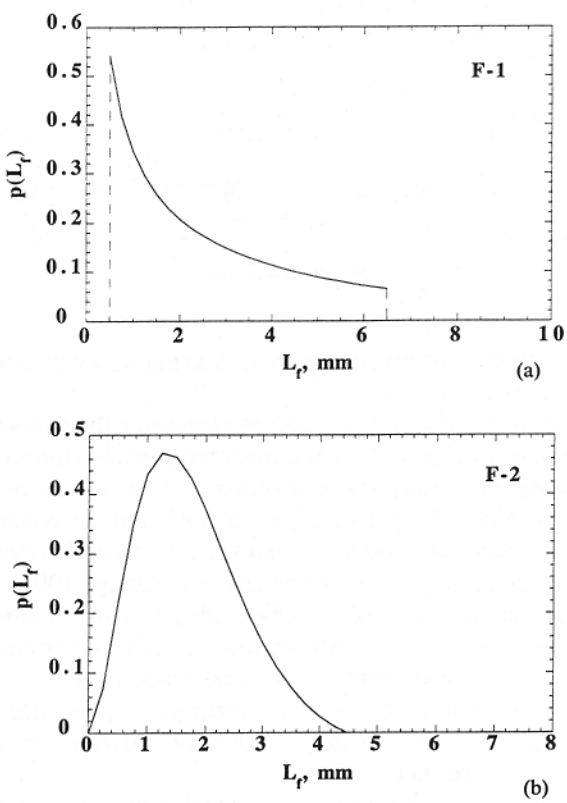

Fig. 9. Probability density functions of measured fiber length distributions after mixing of fibers: (a) F-1, (b) F-2, (c) F-3, (d) F-4, (e) F-5.

Continued overleaf

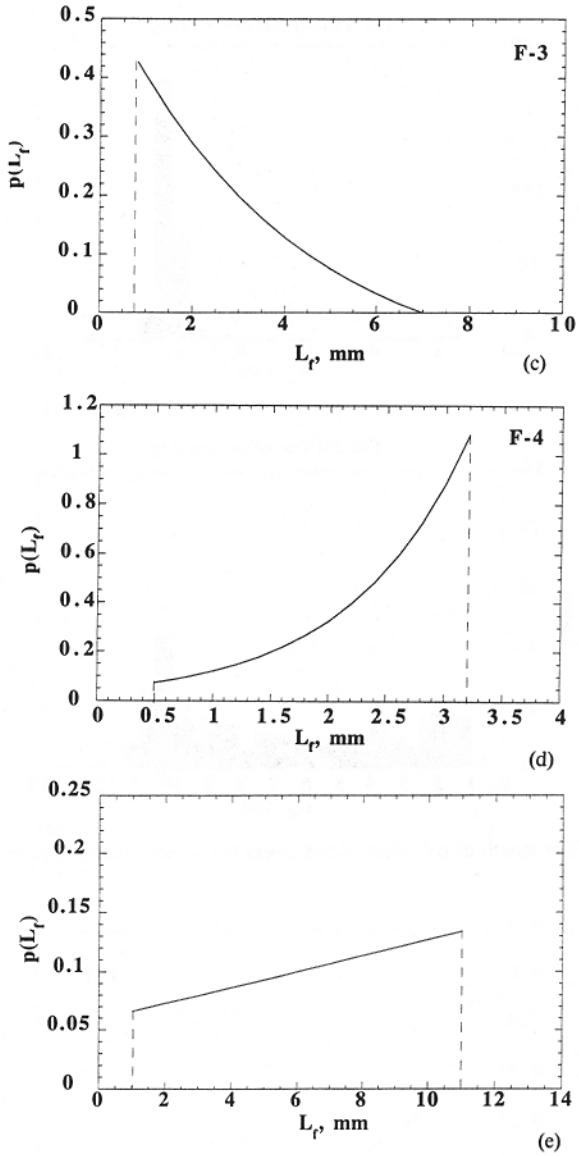

Fig. 9. *continued.*

3. THEORETICAL INVESTIGATION OF COMPOSITE STRESS-CRACK-OPENING RELATION

The composite stress-crack-opening relation represents the stress transferred across a matrix crack due to fiber bridging. This is a macroscopic description of the smeared-out cohesive stress binding the crack faces together and is naturally a function of the magnitude of crack opening. The pre-peak part of such a stress-crack-opening relation is mainly associated with fiber-debonding processes (Li, 1992) and is closely associated with composite pseudo strain-hardening behavior (Li and Leung, 1992; Marshall and Cox, 1988). The post-peak part of the stress-crack-opening relation is closely related to fiber pull-out processes (Li, 1992) and is well known to govern composite fracture energy (Hillerborg, 1980). The micro-mechanics of stress-crack-opening relations for various composites have been under intense studies in recent years (Cox and Marshall, 1991; Li, 1992; Marshall *et al.*, 1985) because they offer opportunities for designing composite properties via micro-structure tailoring.

In the following the composite stress-crack-opening relation for uniform fiber length is briefly reviewed. Extension to the case of composites with fiber length distribution is then presented. This new model is then applied to study the composite ultimate tensile

strength of some of the carbon-fiber cement systems described above. The ultimate tensile strength is identical to the maximum bridging stress in the stress-crack-opening relation when the composite shows pseudo strain-hardening behavior.

3.1.1. *Single fiber load–displacement relation.* Consider a single fiber with an embedded length of ℓ. When the fiber is pulled out, it will initially undergo debonding. Assuming that the fiber–matrix interface is purely frictional in nature (Li and Chan, 1993), the relationship between the fiber bridging load P vs crack opening δ may be obtained from a shear-lag analysis (Li and Leung, 1992):

$$P(\delta)_1 = \frac{\pi}{2}\sqrt{(1+\eta)E_f d_f^3 \tau \delta}\, e^{f\phi} \qquad \text{for} \qquad \delta \leqslant \delta_0 \tag{1}$$

where

$$\delta_0 = (4\ell^2\tau)/[(1+\eta)E_f d_f], \qquad \eta = (V_f E_f)/(V_m E_m).$$

E_f, d_f, V_f, ℓ, τ are the fiber modulus, diameter, volume fraction, embedment length, and fiber–matrix interface bond; E_m, V_m are the matrix modulus and volume fraction; and f is the snubbing coefficient. The snubbing coefficient (Li *et al.*, 1990) can be interpreted as a scale-up factor of the bridging force across a matrix crack when a fiber is pulled out at an inclined angle, analogous to a flexible rope passing over a friction pulley. Specific values of f (typically between 0 and 1) for given fiber/matrix systems can be determined from inclined-fiber pull-out tests.

Subsequent to full fiber debonding, the load-point displacement is mainly due to that of the fiber end slippage. Neglecting the elastic stretching of the fiber, the fiber pull-out load vs displacement relation is given by

$$P(\delta)_2 = \pi\tau\ell d_f\left(1 - \frac{\delta}{\ell}\right) e^{f\phi} \qquad \text{for} \qquad \ell \geqslant \delta \geqslant \delta_0. \tag{2}$$

The fiber bridging force $P(\delta) = 0$ when the fiber completely slides out at $\delta = \ell$.

3.1.2. *Composite bridging stress–displacement relation with uniform fiber length.* Li *et al.* (1991) showed that the composite bridging stress–displacement relation $\sigma(\delta)$ can be predicted by summing the contributions of the individual fibers bridging the matrix-crack plane:

$$\sigma(\delta) = \frac{V_f}{\pi d_f^2/4}\int_0^{\pi/2}\int_0^{(L_f/2)\cos\phi} P(\delta)p(z)p(\phi)\,dz\,d\phi \tag{3}$$

where $p(\phi)$ and $p(z)$ are the probability density functions of the orientation angle and centroidal distance of fibers from the crack plane. For uniform three-dimensional (3-D) random distributions, $p(\phi) = \sin\phi$, and $p(z) = 2/L_f$.

At small crack opening, some fibers will undergo debonding [$P(\delta) = P_1(\delta)$, eqn (1)], while other fibers with short embedment length will undergo slippage [$P(\delta) = P_2(\delta)$, eqn (2)]. Thus using (1) and (2) in (3), the composite bridging stress may be expressed in normalized form (with higher-order terms neglected):

$$\tilde{\sigma}(\tilde{\delta}) = g\left[2\left(\frac{\tilde{\delta}}{\tilde{\delta}^*}\right)^{1/2} - \frac{\tilde{\delta}}{\tilde{\delta}^*}\right] \qquad \text{for} \qquad \tilde{\delta} \leqslant \tilde{\delta}^* \tag{4}$$

where

$$\tilde{\sigma} = \sigma/\sigma_0, \qquad \sigma_0 = V_f\tau(L_f/d_f)/2, \qquad \tilde{\delta} = \delta/(L_f/2), \qquad \tilde{\delta}^* = \left(\frac{2\tau}{(1+\eta)E_f}\right)\left(\frac{L_f}{d_f}\right),$$

and the snubbing factor

$$g = \frac{2}{4+f^2}(1 + e^{\pi f/2}).$$

At crack openings exceeding $\tilde{\delta}^*$ all fibers would have fully debonded and would be in the complete slippage stage. The composite bridging stress may be derived from (3), and together with (2) can be expressed in normalized form:

$$\tilde{\sigma}(\tilde{\delta}) = g(1 - \tilde{\delta})^2 \qquad \text{for} \qquad 1 \geqslant \tilde{\delta} \geqslant \tilde{\delta}^*. \tag{5}$$

The $\tilde{\sigma}(\tilde{\delta})$ is ascending in the region $\tilde{\delta} \leqslant \tilde{\delta}^*$ and descending in the region $1 \geqslant \tilde{\delta} \geqslant \tilde{\delta}^*$ and the value of $\tilde{\delta}^*$ is typically about 0.001 (much less than unity), for typical fiber, matrix and interface parameters in cementitious composites.

The composite $\sigma(\delta)$ relations summarized above assume that the fiber strength will never be exceeded. For the case of fiber rupturing in the composite, the corresponding $\sigma(\delta)$ relations have been developed in Maalej *et al.* (1994) by modifying (1) and (3) to eliminate bridging contributions from ruptured fibers. This is referred to as the Fiber Pull-out and Rupture Model (FPRM) in this paper.

3.2. *Composite bridging stress–displacement relation with variable fiber length*

Due to the observed length variation in carbon fibers, as described in Section 2.4.2 of this paper, the $\sigma(\delta)$ relations are extended to explicitly account for $p(L_f)$ in eqn (3). Hence

$$\sigma(\delta) = \frac{V_f}{\pi d_f^2/4} \int_{L_1}^{L_2} \int_0^{\pi/2} \int_0^{(L_f/2)\cos\phi} P(\delta) p(z) p(\phi) p(L_f)\, \mathrm{d}z\, \mathrm{d}\phi\, \mathrm{d}L_f \tag{6}$$

where L_1 and L_2 represent the shortest and longest fiber length, respectively.

A typical $\sigma(\delta)$ resulting from the present analysis is shown in Fig. 10. The whole curve can be divided into six sectors with different events occurring in each of these sectors. The physical explanation of the events occurring in the different sectors is given here and the detailed governing equations are summarized in the Appendix.

As an overview of the six sectors of the $\sigma(\delta)$ curve, it is useful to keep in mind the four mechanisms of fiber bridging: (1) fiber debonding occurs as a result of activation of an extending friction slip zone on the interface; bridging stress contribution continues to increase with further debonding; (2) fiber rupture occurs when the maximum tensile stress on the fiber exceeds the fiber tensile strength; bridging stress terminates at fiber rupture; (3) fiber sliding occurs when the frictional slip zone extends over the full embedded length of the fiber; bridging stress decreases with further sliding; and (4) at complete slide-out, all further contributions cease.

Thus it is seen that groups of fibers, with different embedment length ℓ, transit from one mechanism to another in the composite, as a result of the matrix crack opening, δ. It is further seen that the cessation of the bridging contribution can be either through fiber rupture or complete slide-out.

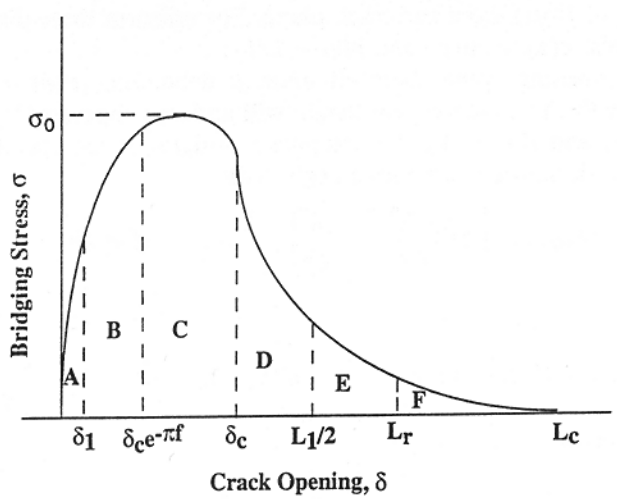

Fig. 10. Schematic $\sigma(\delta)$ relation for composites with variable fiber length.

At any given crack opening, which mechanism a given fiber is undergoing depends on the embedment length of the fiber. Because the fiber stress is raised by the snubbing effect which in turn depends on the inclination angle, ϕ, fiber rupture (or not) will also depend on ϕ. Thus conceptually, it is possible to express

$$\text{Controlling mechanism} = f(\delta, \ell, \phi). \tag{7}$$

This concept is best illustrated by the Fiber Rupture Space Plot (Maalej *et al.*, 1994) shown in Fig. 11. For a fiber with embedment length ℓ and inclination angle ϕ, fiber rupture occurs in the space above the curve defined by

$$\ell_u = L_c e^{-f\phi}$$

where L_c is the conventionally defined critical embedment length given by

$$L_c = \frac{d_f \sigma_{fu}}{4\tau}. \tag{8}$$

Otherwise the fiber will slide out. It is seen that fibers with an embedment length below $L_r = L_c e^{-f\pi/2}$ can never rupture, no matter what inclination angle they have. Further, fibers with an embedment length above L_c will always rupture, even if the inclination angle is zero. It is natural to expect that the embedment length ranges between zero and half the fiber length, so that ℓ is a function of L_f. The present problem is complicated by the fact that $L_1 \leqslant L_f \leqslant L_2$.

The present model assumes $L_1 \leqslant 2L_r \leqslant 2L_c \leqslant L_2$. This implies that short fibers (L_f close to L_1) can pull out, whereas some long fibers (L_f close to L_2) can rupture. If the inequalities are not observed, the model predictions will not be valid. However, it is observed that carbon fibers typically satisfy these assumptions. In the present model, it has further been assumed that carbon fibers suffer no bending rupture in the composite and that they have a uniform strength and diameter. This assumption is likely to be violated by the more brittle fibers with low strain capacity.

3.2.1. *Pre-peak bridging stress-crack-opening relation.*
Sector A ($0 \leqslant \delta \leqslant \delta_1$): In this sector most of the fibers are in the debonding stage. Some fibers with extremely short embedment lengths are in the slipping stage. At $\delta = \delta_1$ all fibers of length L_1 start slipping completely and the equations for $\sigma(\delta)$ or $\tilde{\sigma}(\tilde{\delta})$ governing sector A (see the Appendix) are no longer valid. δ_1 is defined in terms of L_1 by

$$\delta_1 = \frac{\tau L_1^2}{E_f d_f (1 + \eta)}. \tag{9}$$

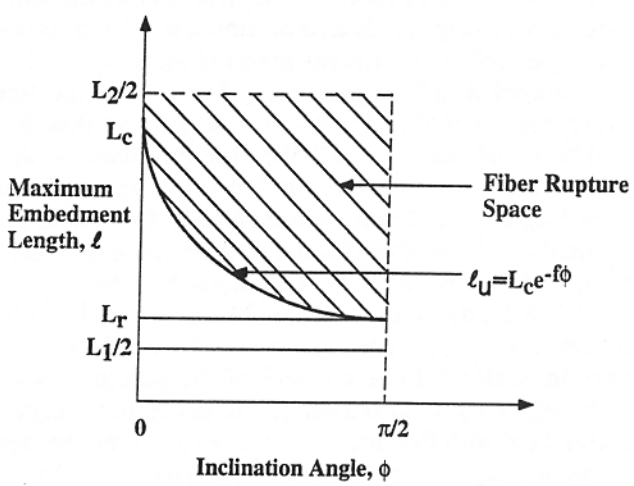

Fig. 11. Fiber rupture space in ℓ–ϕ plot.

Sector B ($\delta_1 \leqslant \delta \leqslant \delta_c e^{-f\pi}$): Once $\delta > \delta_1$, all fibers of length L_1 regardless of their embedment lengths would be completely slipping. With increasing crack opening more and more fibers pass into the complete slipping (no further debonding) stage. Until $\delta = \delta_c e^{-f\pi}$, no fiber ruptures. δ_c is defined by

$$\delta_c = \frac{\sigma_{fu}^2 d_f}{4(1 + \eta)E_f \tau}. \tag{10}$$

(Note: δ and the debond length have a square-root relationship, which explains the factor of this difference in the exponentials of $\delta_c e^{-f\pi}$ and $L_c e^{-f\pi/2}$).

Sector C ($\delta_c e^{-f\pi} \leqslant \delta \leqslant \delta_c$): In this sector fiber rupture begins, starting with those at high inclined angle and with embedment length greater than $L_c e^{-f\pi/2}$. At larger δ, fibers with lower angles will rupture. At δ_c, even fibers normal to the crack plane will rupture.

3.2.2. *Post-peak bridging stress-crack-opening relation.*

Sector D ($\delta_c \leqslant \delta \leqslant L_1/2$): Beyond $\delta > \delta_c$, there is no more fiber debonding and rupture. Only those fibers with short embedment length (which therefore cannot rupture) will pull out and hence only their contribution is considered in the bridging load contribution. All fibers of $L_f < 2L_c e^{-f\phi}$ would be in the complete slipping stage. Among fibers of $L_f > 2L_c e^{-f\phi}$, the pull-out contributions of only those fibers for which $\ell < L_c e^{-f\phi}$ should be counted.

Sector E ($L_1/2 \leqslant \delta \leqslant L_r$): Beyond $\delta > L_1/2$, fibers of length L_1 would have completely pulled out and will no longer contribute to the crack bridging load. As δ continues to increase more and more, fibers of longer length would have completely pulled out and hence their contributions would cease. In this sector the bridging stress contribution comes from two groups: (1) fibers that can never rupture, i.e. $L_1 \leqslant L_f \leqslant 2L_r$, and (2) fibers that could rupture, i.e. $2L_r \leqslant L_f \leqslant L_2$ (but do not rupture as $\ell < L_c e^{-f\phi}$).

Sector F ($L_r \leqslant \delta \leqslant L_c$): As $\delta > L_r$, the bridging stress contributions come from only those fibers with long enough lengths that would cause rupture but did not due to their short embedment length. This corresponds to the second group of fibers mentioned in sector E. The bridging stress σ becomes zero beyond $\delta = L_c$ since long fibers with embedment length less than L_c would have pulled out, and those with embedment length longer than L_c (even if they are aligned normal to the crack plane) must have ruptured.

3.3. *Comparison between model predicted tensile strengths and experimental tensile tests*

The composite tensile strength σ_{cu} predicted by the analytical model is a function of the fiber and interfacial parameters (Table 2). The fiber length distributions $p(L_f)$ used are those measured after mixing (Fig. 9; see also Section 2.4). The interfacial bond strength τ has been estimated by an indirect measurement technique (Obla and Li, 1994). This technique utilizes the measured length of protruding fibers from the fractured composite surface. The resulting τ is reported in Table 2 also. It is found that the bond strength of F-4 fibers is 3.10 MPa as compared to 2.06 MPa for F-5 fibers. Although all the other fiber and matrix parameters are the same, the F-4 fibers have a larger diameter (24 vs 20 μm) and a shorter length (3 vs 10 mm) as compared to F-5 fibers. The larger diameter leads to a smaller number of F-4 fibers (about 30% reduction). This, together with the shorter length, provided better workability. This might have led to a much better matrix packing around the F-4 fibers, thus contributing to the higher bond strength. The snubbing friction coefficient, f, has been assumed to be equal to 0.5.

It was explained in Section 3.2 that the peak of the $\sigma(\delta)$ curve would be equal to the composite tensile strength only when the composite undergoes pseudo strain hardening. Only composites reinforced with F-5 fibers showed pseudo strain hardening (Fig. 1), with those using F-4 showing marginal strain-hardening behavior, and so the tensile strengths for those two composites only are used.

Table 3. Comparisons of tensile strength predictions from analytical models with experimental results

Fiber	L_f (mm)	Bond strength τ (MPa)	FPRM$_1$ model σ_{cu} (MPa)	FRPM$_2$ model σ_{cu} (MPa)	Present model σ_{cu} (MPa)	Experimental σ_{cu} (MPa)
F-4	3	3.10	8.40	7.73	7.19	7.10
		2.78	8.09	7.37	6.80	5.40
F-5	10	2.06	9.98	9.51	8.80	8.20
		1.76	9.82	9.26	8.14	6.20

FPRM$_1$—L_f based on manufacturer's specifications.
FPRM$_2$—L_f based on mean value of measured distribution after mixing, i.e. L_f^{am}.

Table 3 shows a comparison of model predictions with experimentally determined ultimate tensile strengths. Composite strength and fracture surfaces from two specimens were used for each fiber type. The composite tensile strengths were predicted by the original FPRM model in which all fiber lengths were assumed to be equal to that provided in the manufacturers specifications (FPRM$_1$). Then the composite tensile strengths were predicted using the newly developed analytical model described above. It can be easily seen that the newly developed analytical model which assumes the correct fiber length distribution gives more accurate tensile strength predictions. An additional calculation was done by using the original FPRM model but using the mean value of the measured fiber length variation. The result (FPRM$_2$, Table 3) suggests that, at least in those cases, the FPRM model is not unreasonable as a rough estimation tool in predicting the composite tensile strength when the mean fiber length is used.

4. MODEL IMPLICATIONS

The accuracy of the FPRM model using a mean fiber length depends on a number of factors. As expected, it becomes more accurate when the fiber length distribution is limited. Another interesting factor relates to the interfacial bond strength. This is illustrated in Fig. 12, which shows the predicted tensile strength as a function of bond strength using the FPRM model with mean fiber length and the present model accounting for the actual fiber length distribution. The fiber parameters used in this calculation correspond to those for F-3 fibers. It can be seen that the difference in tensile strength predictions is about 10% at a bond strength of 1.5 MPa and rises to about 15% at a bond strength of 2 MPa. As the bond strength is further increased the difference in tensile strength predictions reduces and is about 7% at a bond strength of 5 MPa. The snubbing friction coefficient, f, was assumed to be 0 for these calculations. If f were assumed to be 0.5 (expected of carbon-fibers), then the difference in tensile strength predictions is lower, remaining within 10% at the range of τ shown. The improvement in accuracy of the FPRM model at the high and low end range of τ appears to be a result of a more uniform

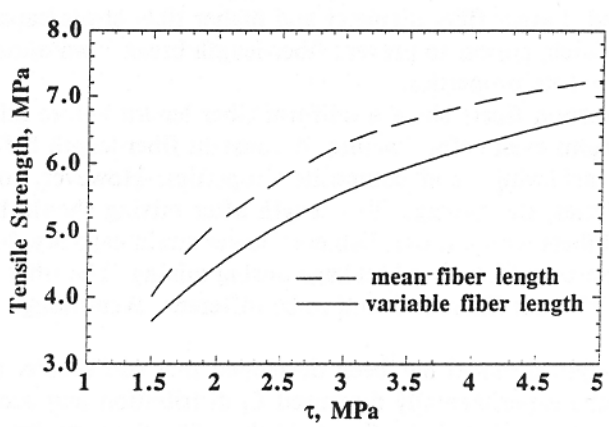

Fig. 12. Composite tensile strength computed for different bond strengths by the FPRM model (dashed line) assuming a mean fiber length, and by the present model (solid line) assuming the actual fiber length distribution.

mode of fiber contribution to composite bridging stress. When τ is small, most fibers are expected to slide out. When τ is large, most fibers are expected to rupture. In the latter case, fiber length becomes immaterial. It is also found that for intermediate bond strengths and high L_2/L_1 ratios [practically possible fiber parameters and $p(L_f)$s] the difference in the composite tensile strength prediction could be as high as 25%.

Figure 13 shows the pre-peak $\sigma(\delta)$ relation for a composite prepared with F-3 fiber parameters using the two different models. The pre-peak part of the $\sigma(\delta)$ relation provides valuable information for the design of pseudo strain-hardening behavior in brittle-matrix composites (Li and Leung, 1992; Marshall and Cox, 1988). An error in accurately predicting this part of the $\sigma(\delta)$ relation would result in an inaccurate prediction of first crack strength and pseudo strain-hardening parameters. This would result in improper design of carbon-fiber cement composites.

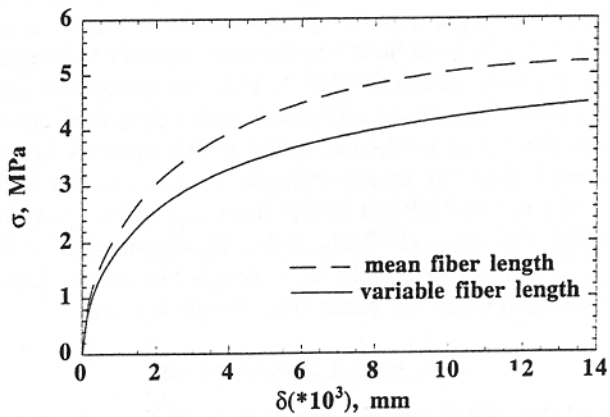

Fig. 13. Pre-peak $\sigma(\delta)$ computed by the FPRM model (dashed line) assuming a mean fiber length, and by the present model (solid line) assuming the actual fiber length distribution.

5. CONCLUSIONS

(1) A database of uniaxial tensile stress–strain relations has been created using a variety of commercially available carbon fibers. It is found that these carbon fibers, with a wide range of properties, produce cement composites with significantly different properties. It is demonstrated that composites with tensile strengths four times higher than plain cement paste (8 vs 2 MPa) and a ductile failure mode with a failure strain capacity 90 times higher (0.90 vs 0.01%) can be achieved.

(2) Carbon fibers with high modulus and strength, often regarded as high-performance fibers in fiber-reinforced polymeric composites, may not necessarily produce the best properties in cementitious composites, particularly when improved composite ductility is desired. Larger fiber diameter and higher fiber-strain capacity, despite lower strength and modulus, appear to prevent fiber-length breakdown during mixing and lead to improved composite properties.

(3) Some carbon fibers show a uniform fiber length before mixing. Others show variable fiber lengths even before mixing. A constant fiber length before mixing is not a requirement for achieving good composite properties. However, to achieve desirable composite properties, the average fiber length after mixing should be maintained at a sufficient level. Fibers with a lower diameter, lower strain capacity, higher modulus and longer length tend to suffer more breakage during mixing. The fiber length distribution after mixing of different fibers is found to be different, even though the mixing process is kept the same.

(4) An analytical model has been developed that can predict the composite $\sigma(\delta)$ curve based on the experimentally measured L_f distribution and accounting for tensile rupture. The model-predicted tensile strengths of carbon-cement composites which undergo strain hardening have been found to agree well with limited experimental results. It is also found that the FPRM model can produce reasonably accurate results provided

the average fiber length measured *after mixing* is utilized. However, for intermediate bond-strength values and high L_2/L_1 ratios the present model should be used in predicting composite strengths accurately.

Acknowledgements—This research was supported by a contract with the Conoco Inc. Discussions with Drs J. McConaghy and A. Katz have been helpful.

REFERENCES

Akihama, S., Kobayashi, M., Suenaga, T., Nakagawa, H. and Suzuki, K. (1986). Mechanical properties of carbon fiber reinforced cement composite and the application to buildings. KICT Report No. 65, Kajima Corporation, Tokyo 182, Japan.

Akihama, S., Suenaga, T. and Banno, T. (1984). Mechanical properties of carbon fiber reinforced cement composite and the application to large domes. KICT Report No. 53, Kajima Corporation, Tokyo 182, Japan.

Banthia, N. (1992). Pitch-based carbon fiber reinforced cements: structure, performance, applications, and research needs. *Can. J. Civ. Engng* **19**, 26–38.

Banthia, N., Moncef, A., Chokri, K. and Sheng, J. (1994). Micro-fiber reinforced cement composites Part I: Uniaxial tensile response. *Can. J. Civ. Engng*, December.

Cox, B. N. and Marshall, D. B. (1991). The determination of crack bridging forces. *Int. J. Fracture* **49**, 159–176.

Ermolenko, I. N., Lyubliner, I. P. and Gulko, N. V. (1990). *Chemically Modified Carbon Fibers and Their Applications*. VCH, New York.

Hillerborg, A. (1980). Analysis of fracture by means of the fictitious crack model, particularly for fibre reinforced concrete. *Int. J. Cement Compos.* **2**(4), November.

Kelly, A. and Macmillan, N. H. (1986). *Strong Solids*, 3rd Edn. Clarendon Press, Oxford.

Li, V. C. (1992). Post-crack scaling relations for fiber reinforced cementitious composites. *J. Mater. Civil Engng* **4**(1), 41–57.

Li, V. C. and Chan, Y. W. (1994). Determination of interfacial debond mode for fiber reinforced cementitious composites. *ASCE J. Engng Mech.* **120**(4), 707–719.

Li, V. C. and Leung, K. Y. (1992). Steady state and multiple cracking of short random fiber composites. *ASCE J. Engng Mech.* **118**(11), 2246–2264.

Li, V. C., Wang, Y. and Backer, S. (1990). Effect of inclining angle, bundling, and surface treatment on synthetic fiber pull-out from a cement matrix. *J. Composites* **21**(2), 132–140.

Li, V. C., Wang, Y. and Backer, S. (1991). A micromechanical model of tension softening and bridging toughening of short random fiber reinforced brittle matrix composites. *J. Mech. Phys. Solids* **39**(5), 607–625.

Li, V. C., Wu, H. C., Maalej, M., Mishra, D. K. and Hashida, T. (1994). Tensile behavior of engineered cementitious composites with discontinuous random streel fibers. *J. Am. Ceram. Soc.* (submitted).

Linton, J. R., Berneburg, P. L., Gartner, E. M. and Bentur, A. (1991). Carbon fiber reinforced cement and mortar. *Materials Research Society Symp. Proc.* Vol. 211, pp. 255–264. Materials Research Society.

Maalej, M., Li, V. C. and Hashida, T. (1994). Effect of fiber rupture on tensile properties of short fiber composites. *ASCE J. Engng Mech.* (submitted).

Marshall, D. B. and Cox, B. N. (1988). A *J*-integral method for calculating steady state matrix cracking stresses in composites. *Mech. Mater.* **7**, 127–133.

Marshall, D. B., Cox, B. N. and Evans, A. G. (1985). The mechanics of matrix cracking in brittle-matrix fiber composites. *Acta Metall.* **33**, 2013–2021.

Nishioka, K., Yamakawa, S. and Shirakawa, K. (1986). Properties and applications of carbon fibre reinforced cement composites. *Proc. RILEM Symp.*

Obla, K. H. and Li, V. C. (1994). A novel technique for fiber–matrix bond strength determination for rupturing fibers (in preparation).

Park, S. B. and Lee, B. I. (1993). Mechanical properties of carbon-fiber-reinforced-polymer-impregnated cement composites. *Cement Concrete Compos.* **15**, 153–163.

Yang, X. and Chung, D. D. L. (1992). Latex-modified cement mortar reinforced by short carbon fibres. *Composites* **23**(6), 453–460.

APPENDIX. COMPLETE $\sigma(\delta)$ RELATION

Based on eqn (6), and the consideration of fiber groups contributing to composite bridging in various sectors (Sections 3.2.1 and 3.2.2), the complete $\sigma(\delta)$ relation can be derived:

Sector	$\sigma(\delta)$	Range
A	$k_1(0, \pi/2, L_1, L_2, 0, \hat{z}_0) + k_2(0, \pi/2, L_1, L_2, \hat{z}_0, h)$	$0 \leqslant \delta \leqslant \delta_1$
B	$k_2(0, \pi/2, L_1, L_f', 0, h) + k_1(0, \pi/2, L_f', L_2, 0, \hat{z}_0) + k_2(0, \pi/2, L_f', L_2, \hat{z}_0, h)$	$\delta_1 \leqslant \delta \leqslant \delta_c e^{-f\pi}$
C	$k_2(\phi_1, \pi/2, L_1, 2L_d, 0, h) + k_2(0, \phi_1, L_1, L_f', 0, h) + k_1(0, \phi_1, L_f', L_2, 0, \hat{z}_0) + k_2(0, \phi_1, L_f', L_2, \hat{z}_0, h) + k_2(\phi_1, \pi/2, 2L_d, L_2, \hat{z}_1, h)$	$\delta_c e^{-f\pi} \leqslant \delta \leqslant \delta_c$
D	$k_2(0, \pi/2, L_1, 2L_d, 0, h) + k_2(0, \pi/2, 2L_d, L_2, \hat{z}_1, h)$	$\delta_c \leqslant \delta \leqslant L_1/2$
E	$k_2(0, \pi/2, 2\delta, 2L_d, 0, h) + k_2(0, \pi/2, 2L_d, L_2, \hat{z}_1, h)$	$L_1/2 \leqslant \delta \leqslant L_r$
F	$k_2(0, \phi_2, 2\delta, 2L_d, 0, h) + k_2(0, \pi/2, 2L_d, L_2, \hat{z}_1, h)$	$L_r \leqslant \delta \leqslant L_c$

where

$$k_1(a,b,c,d,x,y) = \frac{4V_f}{\pi d_f^2}\int_a^b\int_c^d\int_x^y P(\delta)_1 \sin\phi p(L_f)\,dz'\,dL_f\,d\phi$$

$$k_2(a,b,c,d,x,y) = \frac{4V_f}{\pi d_f^2}\int_a^b\int_c^d\int_x^y P(\delta)_2 \sin\phi p(L_f)\,dz'\,dL_f\,d\phi$$

$$\hat{\delta} = \frac{\tilde{\delta}}{\tilde{\delta}^*}, \qquad \hat{z}_0 = z_0\cos\phi, \qquad \hat{z}_1 = z_1\cos\phi, \qquad L_d = L_c\,e^{-f\phi}, \qquad h = \left(1 - \frac{2\delta}{L_f}\right)\cos\phi$$

$$z_0 = 1 - \left[\left(\frac{E_f}{\tau}\right)\left(\frac{d_f}{L_f}\right)\tilde{\delta}\right]^{1/2}, \qquad z' = z/(L_f/2), \qquad z_1 = \left(1 - \frac{2L_c}{L_f}e^{-f\phi}\right)$$

$$L_f' = \left(\frac{E_f d_f \delta(1+\eta)}{\tau}\right)^{1/2} = L_f^*\left(\frac{\tilde{\delta}}{\tilde{\delta}^*}\right)^{1/2}, \qquad \phi_1 = -\frac{1}{2f}\log\left(\frac{E_f d_f \delta}{4L_c^2\tau}\right), \qquad \phi_2 = -\frac{1}{f}\log\left(\frac{\delta}{L_c}\right)$$

$$\tilde{\delta}^* = \left(\frac{2\tau}{(1+\eta)E_f}\right)\left(\frac{L_f^*}{d_f}\right), \qquad L_f^* = \text{Average fiber length from } p(L_f) = \int_{L_1}^{L_2} p(L_f)\,dL_f.$$

Sector	$\bar{\sigma}(\delta)$	Range
A	$g[2(\hat{\delta})^{1/2}f_1(L_1,L_2) - L_f^*\hat{\delta}f_2(L_1,L_2)]$	$0 \le \delta \le \delta_1$
B	$g\left[2(\hat{\delta})^{1/2}f_1(L_f',L_2) - L_f^*\hat{\delta}f_2(L_f',L_2) + \frac{1}{L_f^*}f_3(L_1,L_f')\right]$	$\delta_1 \le \delta \le \delta_c e^{-f\pi}$
C	$G(\phi_1)[2(\hat{\delta})^{1/2}f_1(L_f',L_2) - L_f^*\hat{\delta}f_2(L_f',L_2)] + \frac{g}{L_f^*}f_3(L_1,L_2) - \frac{G(\phi_1)}{L_f^*}f_3(L_f',L_2) - \frac{8}{L_f^*}f_4\left(\phi_1,\frac{\pi}{2},2L_d,L_2\right)$	$\delta_c e^{-f\pi} \le \delta \le \delta_c$
D	$\frac{g}{L_f^*}f_3(L_1,L_2) - \frac{8}{L_f^*}f_4\left(0,\frac{\pi}{2},2L_d,L_2\right)$	$\delta_c \le \delta \le L_1/2$
E	$\frac{g}{L_f^*}f_3(2\delta,L_2) - \frac{8}{L_f^*}f_4\left(0,\frac{\pi}{2},2L_d,L_2\right)$	$L_1/2 \le \delta \le L_r$
F	$\frac{g}{L_f^*}f_3(2\delta,L_2) - \frac{8}{L_f^*}f_4\left(0,\frac{\pi}{2},2L_d,L_2\right) - \frac{1}{L_f^*}f_5\left(\phi_2,\frac{\pi}{2},2\delta,2L_d\right)$	$L_r \leqslant \delta \leqslant L_c$

where

$$f_1(x,y) = \int_x^y p(L_f)\,dL_f$$

$$f_2(x,y) = \int_x^y \frac{p(L_f)}{L_f}\,dL_f$$

$$f_3(x,y) = \int_x^y \left(\sqrt{L_f} - \frac{\tilde{\delta}L_f^*}{\sqrt{L_f}}\right)^2 p(L_f)\,dL_f$$

$$f_4(a,b,x,y) = \int_a^b\int_x^y \left[\frac{L_f}{2}\left(z_1 - \frac{z_1^2}{2}\right) - \frac{\tilde{\delta}z_1 L_f^*}{2}\right]\sin\phi\cos\phi\,e^{f\phi}p(L_f)\,dL_f\,d\phi$$

$$f_5(a,b,x,y) = \int_a^b\int_x^y \left(\sqrt{L_f} - \frac{\tilde{\delta}L_f^*}{\sqrt{L_f}}\right)^2 \sin\phi\cos\phi\,e^{f\phi}\,p(L_f)\,dL_f\,d\phi$$

$$G(\phi_1) = \frac{2}{(4+f^2)}\left(1 - e^{f\phi_1}\cos(2\phi_1) + \frac{e^{f\phi_1}f\sin(2\phi_1)}{2}\right).$$